ELSEVIER

Journal of Chromatography A, 869 (2000) 319–328

JOURNAL OF CHROMATOGRAPHY A

www.elsevier.com/locate/chroma

Analysis of channel-geometry effects on separation efficiency in rectangular-capillary electrochromatography columns

Xiang Zhang, Fred E. Regnier*

Department of Chemistry, Purdue University, West Lafayette, IN 47907-1393, USA

Abstract

A three-dimensional random walk model was developed to evaluate the impact of column geometry on separation efficiency in chromatography systems driven by electroosmotic flow. Contributions of injection plug length, cross-sectional area of channels, and aspect ratio of rectangular channels were examined in these simulation studies. Sample plug length had no impact on efficiency until it exceeded roughly 0.4% of the channel length. Plate height increased rapidly with increasing k' as expected, almost doubling in going from $k'=0.25$ to 0.35. Channel geometry also had a major effect on efficiency. Plate height increased sharply in rectangular channel columns until the channel aspect ratio reached 4–8. But the effect of channel depth was even more dramatic. Minimum plate height (H_{min}) was roughly half that of the channel depth in ideal cases. H_{min} in a 10×2 μm channel was at 1.6 mm s^{-1}. Rectangular channels comparable to those obtained by microfabrication are equivalent to packed column capillary electrochromatography columns in all cases.

Keywords: Efficiency; Electrochromatography; Random walk model; Column geometry; Capillary columns

1. Introduction

There is great interest today in microfabricated separation systems on chips [1–4]. A frequent question is how these systems relate to conventional column technology in terms of efficiency. As opposed to the cylindrical channels in open tubular capillaries, channels in microfabricated systems are trapezoidal or rectangular in cross section. Having one axis larger than the other raises the question of whether this will impact either efficiency or some operational parameter of the system. Theoretical analyses with capillary zone electrophoresis (CZE) have shown that even when the major cross sectional axis is 10–100-times that of the minor there will be no loss in efficiency until the minor axis is so large the capillary has trouble dissipating Joule heat [5]. In this case, thermal effects compromise efficiency. There has also been concern over injection efficiency in chips. Again theoretical analyses of electrokinetic focusing and injection at channel junctions show there is no problem [6,7]. In fact, smaller sample ''plugs'' can be injected in chips and shorter columns can be used.

Liquid chromatographic separations are also of interest in the chip format [8–12]. Because mobile phase mass transfer is known to be much more important in liquid chromatography (LC) than CZE, the issue of whether greater diffusion path length along the lateral axis of microfabricated channels will compromise efficiency arises again. A comparison of the separation efficiency in cylindrical and rectangular capillaries of the same cross sectional

*Corresponding author. Tel.: +1-317-4941-648; fax: +1-317-4940-359.

0021-9673/00/$ – see front matter
PII: S0021-9673(99)01022-5

area has shown that in this special case rectangular capillaries will be of slightly higher efficiency [13,14]. The crucial issue of the impact of capillary geometry on separation efficiency when the channel width is held constant in the range of 2 μm has not been examined. It is critical in LC systems that channel width be <2 μm to minimize mobile phase mass transfer limitations. It is the objective in this paper to develop an algorithm for evaluating the separation efficiency of open tubular capillaries that will allow the relationship between capillary geometry and efficiency to be examined. This will be done through a simulation model of random walk transport.

2. Theory

Separation efficiency in liquid chromatography columns is generally analyzed with models originating from the work of van Deemter et al. [15] and Giddings [16] dealing with packed columns. Neither of these models addresses contributions of column geometry to efficiency. Fortunately, fluid dynamics and analyte transport is considerably simpler in open tubular capillaries than packed columns. Fluid flow is much more streamlined and there is a general absence of stagnant mobile phase mass transfer limitations in capillaries. This lead to the efforts described below to develop a random walk algorithm that describes the chromatographic process as a summation of the paths of individual molecules through a column.

The basic random walk algorithm developed for these studies is as follows. Initially, a predetermined number of molecules are randomly distributed in a loading zone defined in cross section by the geometry of the separation channel and in length by being some multiple of channel width, generally two. Flow at constant velocity is then initiated in the capillary for a predetermined time increment. At the end of this time increment, flow was interrupted and the migration position of each analyte molecule calculated based on the following assumptions. One was that liquid transport was due to electroosmosis and migration velocity was thus identical at all point across the lateral axes of the capillary. A second was that the analytes were neutral and swept through the system at the velocity of the mobile phase, i.e., there was no electrophoretic mobility component to their migration. A third was that all analytes were point-like in dimensions and did not interact with mobile phase constituents. Another assumption was that at the beginning of each migration increment, analyte molecules started from known, but potentially different positions. Still another was that binding and desorption of analytes was totally random. The possibility of competition or displacement was not considered. And finally, it was assumed that zeta potential at sorbent surfaces did not impact the absorption process.

The new position of each analyte molecule at the end of each time increment was calculated using two transport components; that from electroosmotic flow (EOF) alone and the other from random diffusion. This incremental transport process was repeated until all molecules reached the detection region. During this process, boundary conditions were applied whenever there was a collision or interaction between molecules and the stationary phase at the wall. The simulation at the end of each time increment followed a serial process; computation of position on the basis of EOF transport, evaluation of dispersion by diffusion, and analysis of the interaction with stationary phase when the molecule is computed to be at the channel wall. After the simulation at the end of each time increment, the molecular population was summed in discrete segments of time (or distance) and smoothed by the Levenberg–Marquardt method [17].

2.1. Diffusion

Molecular diffusion was simulated using a three-dimensional random walk algorithm. Each dimension was assumed to be fully independent. The probability function of molecular diffusion step length in each time increment of all molecules was derived from the Gaussian profile:

$$P = (2\pi\sigma^2)^{-1/2} \exp[-(\rho - m)^2/2\sigma^2] \quad (1)$$

where ρ is the diffusion step length in each time increment (δt) and σ^2 is standard variance (given by the Einstein–Smoluchoswsi equation [18]), and m is

the most probable diffusion step length. The term m is defined as follow [19]

$$m = (4D\delta t)^{1/2} \quad (2)$$

where D is diffusion coefficient. The diffusion algorithm was implemented by first randomly selecting the diffusion step length traveled by each molecule during the time increment (δt) using the probability distribution in Eq. (1) and then randomizing the direction of migration across the Cartesian coordinates (x, y, z). At the end of each time increment the position of each molecule is recorded and used in the simulation for the next time increment. This process is repeated until all molecules reach the end of the column.

The variance for 10 000 molecules was monitored as a function of simulation time in an effort to verify the diffusion algorithm. All molecules were considered to be totally free in solution, i.e., they did not interact with the wall. The simulated results were compared with predictions based on the Einstein–Smoluchowski equation [18]. As seen in Fig. 1, good agreement is observed for diffusion coefficients in the range of 10^{-4} to 10^{-8} cm^2 s^{-1} using a time increment of 0.1 ms. A similar result was obtained for time increment of 1.0 ms, and time increment of 1.0 ms was chosen in most of the simulation studies reported here to manage computation time. The exception was when desorption time from the stationary phase was very short. In this case a time increment of 0.1 ms was used to allow the probability distribution of diffusion step length to still have a Gaussian profile.

2.2. Electroosmotic transport

EOF results from the formation of an ionic double layer at capillary walls. When voltage is applied across a length of capillary this ionic layer moves and liquid in the capillary is swept along. A theoretical examination of EOF in cylindrical capillaries [20] has concluded that velocity is virtually constant at all points across the radial axis. The flat profiles of EOF in both cylinder and rectangular capillaries have also been visualized [21,22]. Therefore, uniform zeta potential and electroosmotic flow are assumed throughout the system. Although flow at the walls is zero, capillary dimensions are on the order of micrometers whereas the thickness of the double

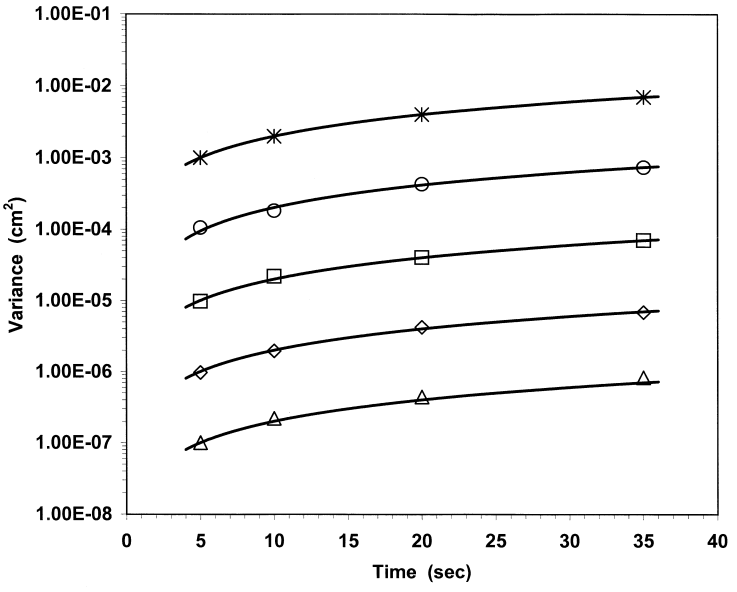

Fig. 1. A comparison of the Einstein–Smoluchowski and three-dimensional random walk methods of evaluating diffusion. The solid line is a plot of variance predicted by the Einstein–Smoluchowski equation [16]. The symbols are values obtained by simulation with analyte diffusion coefficient values of (△) 10^{-8} cm^2 s^{-1}; (◊) 10^{-7} cm^2 s^{-1}; (□) 10^{-6} cm^2 s^{-1}; (○) 10^{-5} cm^2 s^{-1}; and (*) 10^{-4} cm^2 s^{-1}.

layer is on the order of the Debye radius which is only a few nanometers. This also means that in chromatographic systems with the stationary phase at the capillary wall, molecules will not pass a mobility interface when they pass between the mobile and stationary phase.

2.3. Retention

Kinetics of the chromatographic partitioning process is frequently described in terms of the constant K

$$K = \langle t_d \rangle / \langle t_a \rangle \tag{3}$$

where $\langle t_d \rangle$ is the average time required for an analyte to desorb from the stationary phase and $\langle t_a \rangle$ is the average time required for absorption per unit length of column. In addition to being connected to temperature, interfacial surface area, and mobile phase viscosity, this constant is also strongly related to bonding energy [16]. At a macroscopic level, chromatographic migration rate is often expressed in terms of a capacity factor (k') in which

$$k' = N_s / N_m = t_s / t_m \tag{4}$$

where N_s is the number of moles of analyte in the stationary phase, N_m is number of moles of analyte in the mobile phase, t_s is the time analyte spends in the stationary phase and t_m is the time spent in the mobile phase. These terms may be more specifically related to the physical characteristics of the system by the equation

$$k' = K_d \cdot \frac{A_s}{V_m} = K_d \phi \tag{5}$$

where K_d is the chromatographic distribution coefficient, A_s is the specific surface area of the sorbent, V_m is the specific volume of the mobile phase, and ϕ is the phase ratio. These variables in the case of rectangular channels fabricated by gas phase etching are given by the equations

$$A_s = 2(a + b)L \tag{6a}$$

$$V_m = abL \tag{6b}$$

and

$$\phi = 2(a + b)/ab \tag{6c}$$

where a is the channel depth, b is channel width, and L is channel length.

When a molecule encounters the channel wall it may either be adsorbed into the stationary phase, undergo an elastic collision and be deflected away from the wall back into the mobile phase immediately, or collides and diffusion away in next time increment. The probability that a molecule will undergo a transition to the surface adsorbed state is given as

$$P^j_{m\to s} = \frac{N^j_{m\to s}}{N^j} \tag{7}$$

where $N^j_{m\to s}$ is the number of molecules moving into the adsorbed state during the jth time increment and N^j is the total number of molecules reaching the channel wall during the time increment. According to Eq. (4), $N^j_{m\to s}$ can be given as

$$N^j_{m\to s} = k' N^j_m - N^j_s \tag{8}$$

where N^j_m is the number of molecules remaining in the mobile phase and N^j_s is the number of molecules already adsorbed at the jth time increment. After randomly selecting a number of molecules moving into the adsorbed state, the rest of the molecules reaching the channel wall during the jth time increment are either going to undergo elastic collision or enter the stationary phase. These two possibilities have an equal probability of 0.5. If a molecule passes into the absorbed state, molecular diffusion will occur in two dimensions on the surface until it is again desorbed into the mobile phase. Considering desorption to be a Poisson process [23], desorption time, t_d, is given as

$$t_d = -\langle t_d \rangle \log(\zeta) \tag{9}$$

where ζ is a random number given by a uniform random generator.

In this study, adsorption was considered to be a diffusion controlled process, and $\langle t_a \rangle$ is given as

$$\langle t_a \rangle = 1/N^j_{m\to s} \sum \frac{t^j}{d^j} \tag{10}$$

where t^j is the time the jth molecule spent in the mobile phase after it last departed from the surface and d^j is the distance the jth molecule traveled in the direction of flow during the time period t^j. Combin-

ing Eqs. (3), (5) and (10) and substituting them into Eq. (9) produces a relationship between t_d and k'. Using k' as a free parameter, desorption time (t_d) can be determined. It should be noted that d^j cannot be zero in Eq. (10) even though d^j could equal 0.0 in a three-dimensional random walk process. If this happens, t^j/d^j is given a value to make t_s/t_m fall into a region given $k' \pm 0.005$.

3. Results and discussion

The equations derived above were used to simulate average diffusion time, analyte position, and plate height as a function of linear velocity and analyte diffusion coefficient in channels of different geometry. Analyte was randomly distributed throughout a sample volume of length equal to twice the channel width and identical in cross-sectional geometry to that of the separation channel. Analyte diffusion coefficient in the mobile phase (D_m) was taken to be $1.6 \cdot 10^{-6}$ cm^2 s^{-1} whereas that used in the stationary phase (D_s) was set at $D_m/2$. At least three simulation runs were averaged to determine the effect of a given experimental parameter. Data were also examined at various stages of the simulation process to confirm that separations were proceeding in a logic fashion (data not shown). Computer code used in this study was written in C^{++} using C^{++} Builder 3.0 and was executed on a personal computer with a Pentium II, 333 MHz processor.

A comparison of simulated and experimental data in Fig. 2 shows that they are in good agreement. The extent to which the theoretical and experimental results agree led to the conclusion that the simple random walk model described above is suitable to evaluate the impact of channel geometry on separation efficiency.

3.1. Effect of channel geometry on average diffusion time

The objective of this portion of the study was to examine the impact of channel geometry on the average time taken by a molecule to diffuse to a channel wall. Average diffusion time was calculated by the equation

$$\langle t \rangle = \frac{1}{N \sum t_i} \tag{11}$$

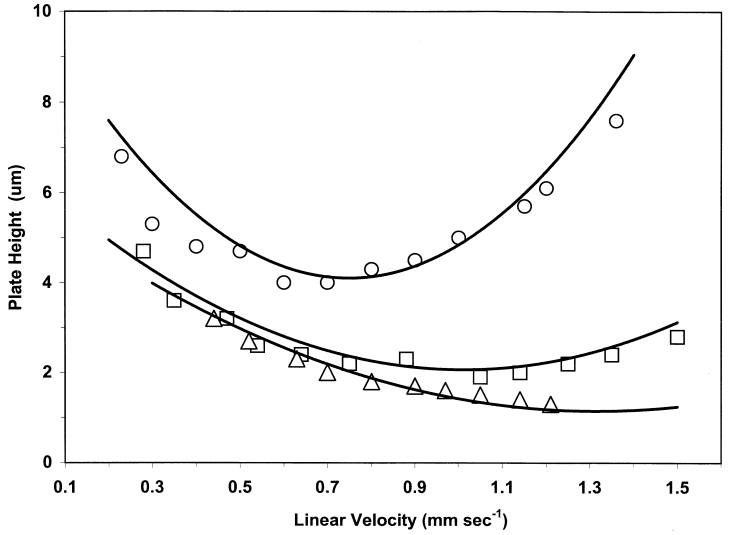

Fig. 2. Plate height curve of simulated and experimental results from open tubular capillary electrochromatography columns. The solid lines were obtained by simulation. The symbols are values for data obtained from the literature [9] with channels of (△) 23×2.9 μm; (□) 33×4.7 μm; and (○) 45×8.7 μm. k' was arbitrarily chosen as 0.2, 0.21 and 0.25 for these three channels, respectively. Values set for other parameters were $N=10^3$, $\delta t=10^{-3}$ s, $D_m=1.6 \cdot 10^{-6}$ cm^2 s^{-1}, $D_s=8 \cdot 10^{-7}$ cm^2 s^{-1} and $L=2.7$ cm.

where N is the total number of molecules being examined and t_i is the time required by the ith molecule to diffuse to the channel wall. Channel geometry is expressed in terms of an aspect ratio, which is defined as the ratio of the length of the maximum lateral axis divided by that of the minor axis. Henceforth the maximum lateral axis will be referred to as the channel width and the minor axis will be described as the channel depth.

Simulations (Fig. 3) show that average diffusion time ($\langle t \rangle$) of an analyte to a channel wall increases sharply as aspect ratio increases, reaching a maximum at aspect ratios of 4–8 with all channel depths. Beyond an aspect ratio of 10 there is no increase in $\langle t \rangle$ at any channel depth. Because channel width is always greater than channel depth in rectangular capillaries, channel depth has the greatest impact on $\langle t \rangle$. When channel depth is 1.5 μm or less, analytes obviously diffuse to the channel walls very quickly without regard to channel ratio. It may be further concluded from this figure that square (aspect ratio of 1) or cylindrical capillaries provide much higher efficiency than rectangular capillaries of the same channel width. Lateral diffusion along the major axis of rectangular capillaries substantially compromises efficiency up to an aspect ratio of 4–8.

3.2. Effect of injection plug length on plate height

Sample may be loaded into microfabricated rectangular channels in two ways. One is known as the floating sample loading method [24–26] and the other is referred to as pinched sample loading or crossed-channel injection [8,26]. The pinched loading scheme is most widely used because it provides greater temporal stability and allows more precise control of plug length [26]. Pinched sample loading was simulated in these studies by assuming sample was loaded into the channel ''cross'' and injected instantaneously, electric field strength was uniformly distributed, and the shape of the plug was identical to that of the channel intersection.

The contribution of injection plug length to plate height (h) in CZE has been estimated in cylindrical capillaries [27] by the equation

$$h = \frac{l^2}{12L} \tag{12}$$

where l is the length of the injected sample and L is the length of the separation channel. It can be seen that smaller injection length will give better efficiency. Simulations (Fig. 4) in the case of mi-

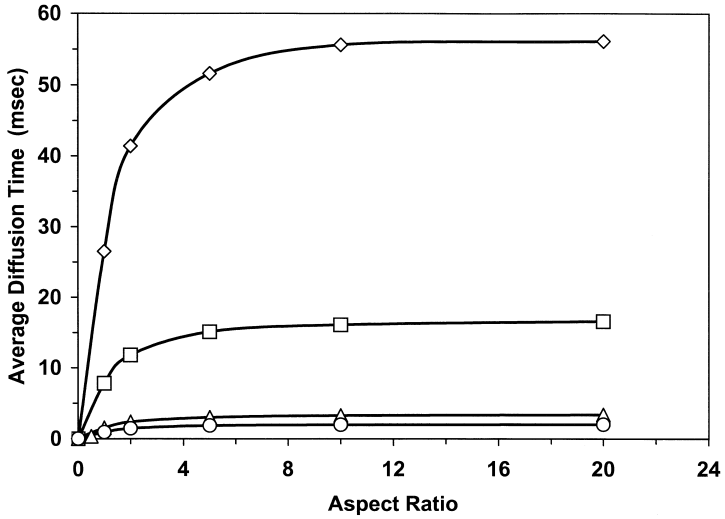

Fig. 3. The average time required for analyte diffusion to channel walls as a function of channel aspect ratio. ○ represents data for a 1.5 μm channel depth; △, 2 μm; □, 5 μm; and ◇, 10 μm. Values set for other parameters were $N=10^4$, $\delta t=10^{-3}$ s and $D_m=10^{-6}$ cm^2 s^{-1}.

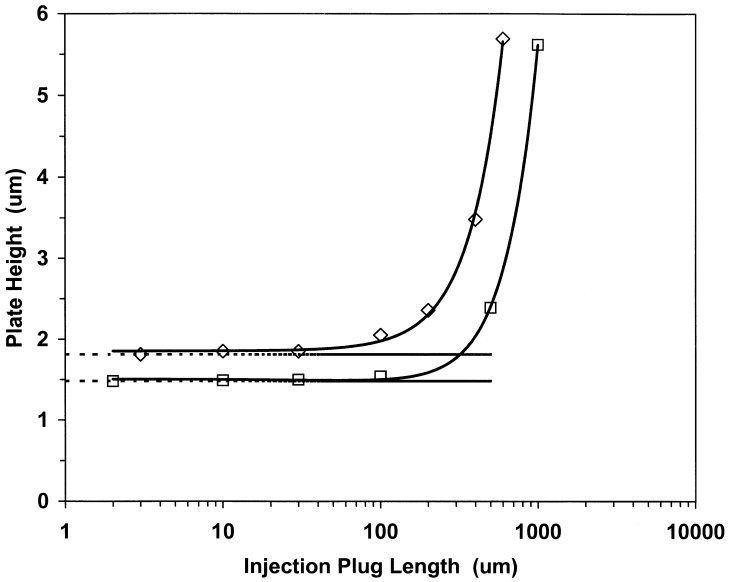

Fig. 4. The effect of sample plug length on system plate height. ◊ represents data for a 1.0 cm channel length; □, 2.7 cm channel length, and dot line is baseline. Values set for other parameters were $N=5\cdot10^3$, $\delta t=10^{-3}$ s, $D_m=1.6\cdot10^{-6}$ cm^2 s^{-1}, $D_s=8\cdot10^{-7}$ cm^2 s^{-1} and $k'=0.25$.

crofabricated channels were undertaken using a 10×2 μm rectangular geometry and separation path lengths of 1.0 and 2.7 cm. The baseline shows the plate height predicted as the injection plug length approaches zero. It is seen in Fig. 4 that plate height increases little beyond the baseline until the injection plug length begins to exceed roughly 0.4% of the column length. This means the maximum injection plug length in the 1.0 and 2.7 cm columns will be 40 and 108 μm, respectively. As injection plug length increases to 4% of the column length, more than 60% of column efficiency is lost in the 1.0 cm column. These observations are similar to those predicted from Eq. (12).

3.3. Effect of capacity factor on plate height

Simulations of plate height (H) as a function of analyte capacity factor (k') in an 45×8.7 μm channel of 2.7 cm length (Fig. 5) show that H increases with k'. This is as expected. The great difference in analyte velocity between the mobile and stationary phases increases zonal dispersion as the analyte spends more time in the mobile phase at high k' values. It is interesting that H doubles with the small change in k' from 0.25 to 0.35.

3.4. Effect of aspect ratio and channel width on plate height

It was noted in Fig. 3 that both channel depth and aspect ratio impacted the average diffusion time ($\langle t\rangle$) of an analyte to channel walls. Whereas $\langle t\rangle$ was proportion to channel depth, increases in $\langle t\rangle$ reached a plateau at aspect ratio greater than 4–8. Having selected optimum injection plug lengths and noted the effect of k' and plate height, it is possible to examine the effect of channel depth and aspect ratio on plate height. At a constant aspect ratio of 5, it is seen in Fig. 6 that the minimum plate height (H_{min}) in a 2 μm deep channel is less than half that of a 4.3 μm channel. Furthermore, H_{min} is achieved at higher linear velocity and plate height still does not exceed 2 μm at 3 mm s^{-1} in the smaller 2 μm deep channel. All of these characteristics are expected and desirable. It should be noted however, that the impact of Joule heating on column efficiency at high mobile phase velocity was not examined in these studies.

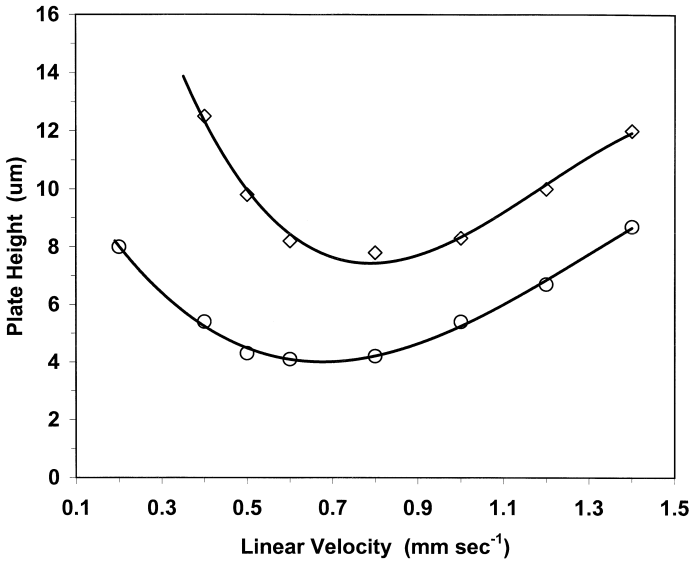

Fig. 5. The effect of capacity factor on plate height. ◊ represents data for $k'=0.35$; ○, $k'=0.25$. Values set for other parameters were $N=5\cdot10^3$, $\delta t=10^{-3}$ s, $D_m=1.6\cdot10^{-6}$ cm^2 s^{-1}, $D_s=8\cdot10^{-7}$ cm^2 s^{-1} and $L=2.7$ cm.

Heat dissipation will also be related to channel geometry. When deeper channels of 8.7 and 22.5 μm are used, plate height and H_{min} increase substantially (Fig. 7), even though a much more favorable aspect ratio of 2 is being used in the case of the 45×22.5 μm channel. These studies confirm the observation

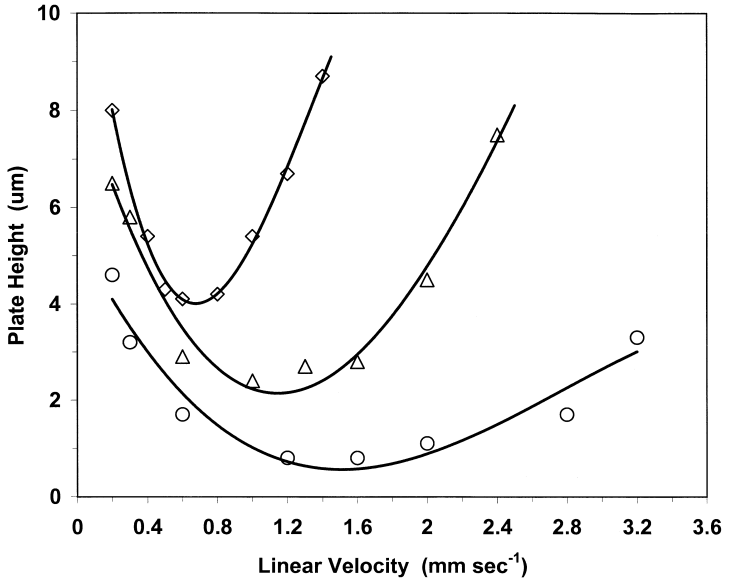

Fig. 6. The impact of channel depth on plate height at a fixed aspect ratio. ○ is for data derived from a 10×2 μm channel; Δ, 22.5×4.3 μm; and ◊, 45×8.7 μm. Values set for other parameters were $N=10^3$, $\delta t=10^{-3}$ s, $D_m=1.6\cdot10^{-6}$ cm^2 s^{-1}, $D_s=8\cdot10^{-7}$ cm^2 s^{-1}, $L=2.7$ cm and $k'=0.25$.

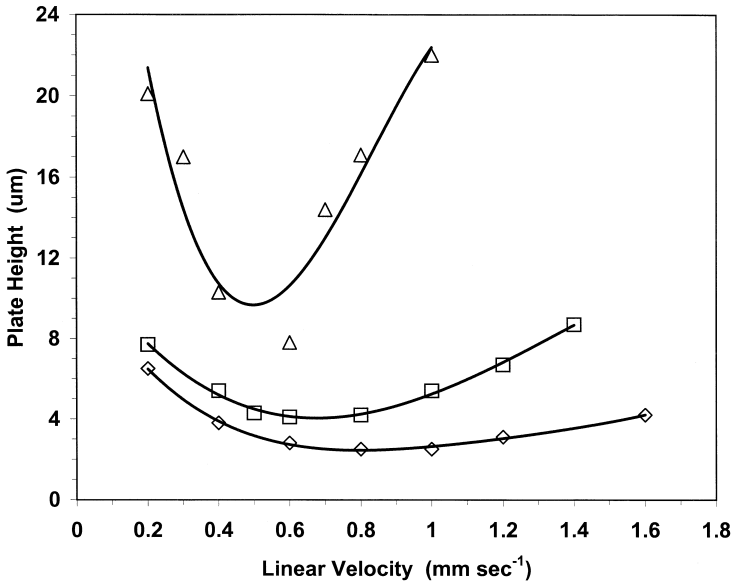

Fig. 7. The effect of aspect ratio on plate height. ◊ is for data derived from a 45×4.3 μm channel; □, 45×8.7 μm; and Δ, 45×22.5 μm channel. Values set for other parameters were $N=10^3$, $\delta t=10^{-3}$ s, $D_m=1.6\cdot10^{-6}$ cm^2 s^{-1}, $D_s=8\cdot10^{-7}$ cm^2 s^{-1}, $L=2.7$ cm and $k'=0.25$.

made in Fig. 3 that channel depth is a dominant issue in the efficiency of microfabricated chromatography columns. It is also worth noting that both the observed efficiencies of microfabricated CEC columns [8] and those predicted in this paper are comparable to the efficiencies of current packed capillary electrochromatography columns.

4. Conclusions

First, it may be concluded that a simple three-dimensional random walk model can be used to evaluate the contribution of geometric parameters, partitioning properties, and analyte diffusion coefficient to the efficiency of chromatography columns when the separation is driven by electroosmotic flow. These studies have shown that it is much easier to examine the impact of sample plug size, viscosity, k', or channel geometry through modeling than by experimentation. The cost and time involved in fabricating a large number of chips of different channel geometry would be large.

Second, it is concluded that rectangular channels provide lower separation efficiency in chromatographic systems than cylindrical channels by allowing oblique diffusion along the major lateral axis of the channel. These mobile phase mass transfer limitations reach a maximum at aspect ratios of 4–8. Most rectangular capillary electrochromatography systems reported in the literature were of equal or greater aspect ratio, meaning they were operating at a point of lowest efficiency.

Third, it is concluded that the separation efficiency of open tubular systems can be comparable to the current generation of packed columns. From the limited data in the literature, it has been seen that the plate height is always less than the channel depth. Simulations presented here indicate that a low k', plate height can be less than half the channel depth. Current fabrication technology can give channels of 1.5–2.0 μm in depth. Although open tubular rectangular channels provide lower efficiency than cylindrical channels, they are still more efficient than current packed columns. Still higher efficiency could be expected if it is possible to fabricate sub-micron depth channels.

Finally, it is concluded that capillary electrochromatography systems with a single channel of 2 μm of less in depth are most likely not practical. They would be difficult to fabricate and even if constructed would be easily plugged by particles or

sample fouling. Some type of capillary bundling of the type used in collocated monolith columns would seem more appropriate. Columns containing 16 to thousands of channels operating in parallel have been produced [1,8,28]. Aspect ratios in these rectangular channel systems have been in the range of 5–7 to maximize path length through the channel for optical detection perpendicular to the face of the chip.

Acknowledgements

The authors gratefully acknowledge financial support from NIH grant number 35421.

References

[1] B. He, F.E. Regnier, J. Pharm. Biomed. Anal. 17 (1998) 925–932.
[2] C.S. Effenhauser, G.J.M. Bruin, A. Paulus, M. Ehrat, Anal. Chem. 69 (1997) 3451–3457.
[3] A.T. Woolley, D. Hadley, P. Landre, A.J. deMello, R.A. Mathies, M.A. Northrup, Anal. Chem. 68 (1996) 4081–4086.
[4] Z.H. Fan, D.J. Harrison, Anal. Chem. 66 (1994) 177–184.
[5] A. Cifuentes, H. Poppe, Chromatographia 39 (1994) 391–404.
[6] N.A. Patankar, H.H. Hu, Anal. Chem. 70 (1998) 1870–1881.
[7] S.V. Ermakov, S.C. Jacobson, J.M. Ramsey, Anal. Chem. 70 (1998) 4494–4504.
[8] B. He, N. Tait, F.E. Regnier, Anal. Chem. 70 (1998) 3790–3797.
[9] J.P. Kutter, S.C. Jacobson, N. Matsubara, J.M. Ramsey, Anal. Chem. 70 (1998) 3291–3297.
[10] A.T. Woolley, K. Lao, A.N. Glazer, R.A. Mathies, Anal. Chem. 70 (1998) 684–688.
[11] F.E. Regnier, B. He, S. Lin, J. Busse, TIBTECH 17 (1999) 101–106.
[12] S. Liu, Y. Shi, W.W. Ja, R.A. Mathies, Anal. Chem. 71 (1999) 566–573.
[13] A. Cifuentes, H. Poppe, Electrophoresis 16 (1995) 2051–2059.
[14] A. Cifuentes, M.A. Rodriguez, F.J. Garcia-Montelongo, J. Chromatogr. A 737 (1996) 243–253.
[15] I.J. van Deemter, F.J. Zuiderweg, A. Klinkenberg, Chem. Eng. Sci. 5 (1956) 271.
[16] J.C. Giddings, Dynamics of Chromatography. Part 1, Principles and Theory, Marcel Dekker, New York, 1965.
[17] W.H. Press, B.P. Flannery, S.A. Teukolsky, W.T. Vetterling, Numerical Recipes – The Art of Scientific Computing, Cambridge University Press, Cambridge, 1989.
[18] A. Einstein, Ann. Phys. 17 (1905) 549.
[19] D.L. Hopkins, V.L. McGuffin, Anal. Chem. 70 (1998) 1066–1075.
[20] C.L. Rice, R. Whitehead, J. Phys. Chem. 69 (1965) 4017–4024.
[21] T. Tsuda, M. Ikedo, J. Chromatogr. 632 (1993) 201–207.
[22] P.H. Paul, M.G. Garguilo, D.J. Rakestraw, Anal. Chem. 70 (1998) 2459–2467.
[23] M.R. Schure, A.M. Lenhoff, Anal. Chem. 65 (1993) 3024–3037.
[24] A. Manz, D.J. Harrison, E.M.J. Verpoorte, J.C. Fettinger, A. Paulus, H. Ludi, H.M. Widmer, J. Chromatogr. 593 (1992) 253–258.
[25] D.J. Harrison, A. Manz, Z. Fan, H. Ludi, H.M. Widmer, Anal. Chem. 64 (1992) 1926–1932.
[26] S.C. Jacobson, R. Hergenroder, L.B. Koutny, R.J. Warmack, J.M. Ramsey, Anal. Chem. 66 (1994) 1107–1113.
[27] J.C. Sternberg, Adv. Chromatogr. 2 (1966) 205.
[28] S. Lin, Ph.D. Thesis, Purdue University, 1999, p. 37.